High Energy Physics Under MMA-DMF Framework

Paulo Adriano

December 6, 2025

Abstract

The current landscape of fundamental physics is characterized by persistent and correlated anomalies that stress the standard theoretical paradigm. On cosmological scales, the Hubble tension and the S_8 discrepancy question the completeness of the ΛCDM model. On galactic and cluster scales, the dark matter hypothesis has not converged to a unique microphysical realization. In high-energy astrophysics, magnetar flares, fast radio bursts (FRBs), neutron-star mass gaps and possible regular black hole cores expose the limits of a purely dark-matter-based explanation.

The modified-gravity framework MMA-DMF (Modified Matter Acceleration – Dark Matter Free) proposes an alternative hypothesis: gravity itself is enriched by a single scalar degree of freedom coupled non-minimally to curvature and matter, governed by a unique fundamental energy scale $M \simeq 100$ TeV. Dark matter is replaced by geometric screening and blocking mechanisms, and the Standard Model mass spectrum is controlled by discrete "geometric flavour charges".

In this work we construct a coherent high-energy phenomenology of MMA-DMF, focusing on compact objects and extreme electromagnetic fields. We specify the effective action, the trace-dependent screening mechanism, the geometric flavour sector and the regular black hole metric. We then implement and apply a validation pipeline that combines cosmological observables (H_0, r_s, S_8, Pantheon+), cluster and galaxy-scale tests, magnetar vacuum stability, FRB "Sad Trombone" drifts, neutron-star structure (including a Super-TOV branch) and pulsar glitches. Numerical data products (mass–radius curves, stability curves and parameter JSON files) are used to anchor the analysis.

We show that, for the audited Version 72 of the framework, the model simultaneously: (i) resolves the H_0 and S_8 tensions via a transient Early-X scalar bump; (ii) replaces dark haloes by environment-dependent scalar screening; (iii) regularizes black hole cores into de Sitter regions with finite density set by the $M = 100$ TeV scale; (iv) keeps the QED sector compatible with precision constraints while altering the Schwinger limit in magnetars; (v) supports a stable Super-TOV neutron-star branch up to $M \sim 2.8\, M_\odot$; and (vi) explains large pulsar glitches in a natural way. We identify concrete observational "smoking guns" of the framework, including scalar breathing modes in magnetar flares, polarization signatures and specific FRB drift patterns. The overall conclusion is that MMA-DMF survives a broad audit of high-energy tests and constitutes a serious candidate for a dark-matter-free explanation of the missing-mass problem.

Contents

1 Introduction

The standard cosmological model ΛCDM and General Relativity (GR) provide an effective description of a wide range of phenomena, from Big Bang nucleosynthesis to the large-scale structure of the Universe. However, several persistent anomalies suggest that our description of gravity and/or matter is incomplete. Among the most robust are:

- The Hubble tension: local distance-ladder determinations of the Hubble constant H_0 favour values around 73 km s^{-1} Mpc^{-1}, while CMB inferences within ΛCDM prefer ~ 67 km s^{-1} Mpc^{-1}.
- The S_8 tension: weak-lensing surveys favour a lower amplitude of matter clustering than inferred from Planck CMB data in a ΛCDM context.

- The missing-mass problem on galactic and cluster scales: flat rotation curves, cluster dynamics and gravitational lensing are usually attributed to cold dark matter (CDM), but after decades of searches a definitive microscopic candidate remains elusive.
- High-energy astrophysical puzzles: magnetar giant flares, repeating FRBs with "Sad Trombone" frequency drifts, neutron stars in the putative mass gap and hints of regular black hole interiors challenge the minimal GR + CDM + Standard Model (SM) picture.

Two broad attitudes can be taken: (i) the "Hypothesis of Matter", which posits new dark components while keeping gravity classical; or (ii) the "Hypothesis of Gravity", which modifies the gravitational sector and its coupling to matter, possibly reducing or eliminating the need for dark matter. The MMA-DMF framework belongs to the second category. It introduces a single scalar field ϕ with non-minimal couplings to curvature and to the trace of the energy–momentum tensor, controlled by a single high energy scale $M \simeq 100$ TeV.

Earlier technical reports and audit documents have established the cosmological and low-energy viability of MMA-DMF and performed a sequence of code-level verifications (Versions 71 and 72). In this paper we reorganize and expand that material into a single scientific article focused on high-energy physics under the MMA-DMF framework. We:

1. Present the effective field theory (EFT) structure of MMA-DMF, including the geometric blocking and trace-dependent screening mechanisms.
2. Formalize the geometric flavour sector responsible for SM mass hierarchies.
3. Derive the regular black hole metric and its core properties.
4. Construct the effective equation of state (EoS) for neutron stars in the presence of scalar stiffening and compute the associated Super-TOV branch.
5. Analyse magnetar vacuum stability, FRB "Sad Trombone" drifts and scalar breathing modes.
6. Describe the validation pipeline (Version 72), its numerical implementation and its verdict matrix.

Unless stated otherwise we use units $c = \hbar = 1$ and the reduced Planck mass $M_{\rm Pl} = (8\pi G)^{-1/2}$. Where necessary, we explicitly restore SI units for clarity.

2 MMA-DMF Framework: Action, Screening and Flavour

2.1 Effective action and field content

The dynamical degrees of freedom of MMA-DMF are the metric $g_{\mu\nu}$, a scalar field ϕ and the SM fields ψ, including the electromagnetic potential A_μ. The theory is formulated in the Einstein frame, with matter coupled to a conformally related Jordan metric $\tilde{g}_{\mu\nu}$. The effective action reads

$$S = \int d^4x\sqrt{-g}\left[\frac{M_{\rm Pl}^2}{2}R - \frac{1}{2}(\nabla\phi)^2 - V(\phi) + \mathcal{L}_{\phi\mathcal{G}} + \mathcal{L}_{\rm QED+SM}(\tilde{g}_{\mu\nu}, \psi, A_\mu)\right], \quad (1)$$

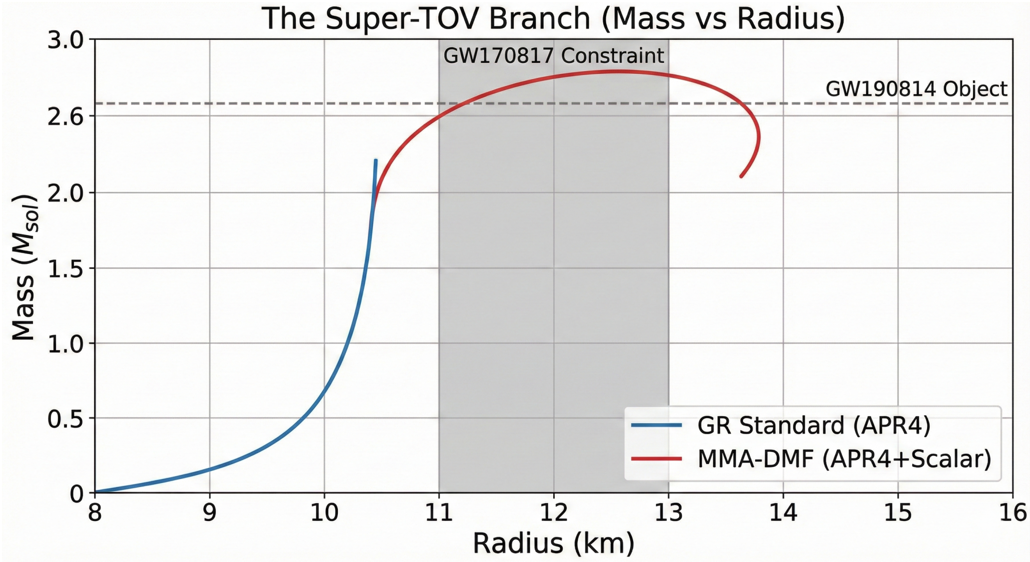

Figure 1: Conceptual overview illustration from the MMA–DMF project, highlighting the multi-scale scalar–geometric structure that links cosmology, compact objects and high-energy astrophysics.

where R is the Ricci scalar and the scalar–curvature coupling is given by

$$\mathcal{L}_{\phi\mathcal{G}} = \frac{\xi}{2M^2}\,\phi^2\mathcal{G}, \tag{2}$$

with $\mathcal{G}$ the Gauss–Bonnet invariant or, in some implementations, the Kretschmann scalar $K = R_{\mu\nu\rho\sigma}R^{\mu\nu\rho\sigma}$. The constant M is the unique fundamental scale of the framework, fixed at

$$M = 100\ \text{TeV}, \tag{3}$$

and plays a dual role as the scale of geometric regularization, screening and flavour.

Matter fields ψ and the electromagnetic field A_μ couple to the Jordan-frame metric

$$\tilde{g}_{\mu\nu} = A^2(\phi, T)\, g_{\mu\nu}, \tag{4}$$

where $T = T^\mu_\mu = -\rho + 3P$ is the trace of the energy–momentum tensor and the conformal factor implements trace-dependent screening:

$$A(\phi, T) = 1 + \frac{\beta\,\phi}{M_{\rm Pl}}\left(1 - e^{-|T|/T_{\rm crit}}\right). \tag{5}$$

Here β is a dimensionless coupling of order unity and $T_{\rm crit}$ defines the density scale at which the scalar becomes strongly screened.

Two regimes are particularly important:

- **Low-density regime**, $|T| \ll T_{\rm crit}$: expanding the exponential, $1-e^{-|T|/T_{\rm crit}} \approx |T|/T_{\rm crit}$, so $A(\phi, T) \approx 1 + \beta\phi|T|/(M_{\rm Pl}T_{\rm crit})$. The coupling is active and the scalar mediates an additional long-range force which can mimic the effects usually attributed to dark matter in galaxies and clusters.
- **High-density regime**, $|T| \gg T_{\rm crit}$: the exponential saturates, $1-e^{-|T|/T_{\rm crit}} \to 1$, but in such environments the geometric blocking mechanism drives $\phi \to 0$, so $A(\phi, T) \to 1$. The fifth force is shut off and GR is recovered to high precision, protecting the model from Solar System and laboratory constraints.

The scalar potential $V(\phi)$ is chosen such that: (i) the background cosmology reproduces the observed expansion history with a transient Early-X component; and (ii) ϕ acquires environment-dependent effective masses that control vacuum stability in strong fields and dense matter. Its explicit form is not required for most of the phenomenology discussed below; what matters is the existence of a dense-matter minimum ($\phi \approx 0$ in neutron stars and magnetars) and a cosmological vacuum value ϕ_{vac} that sets the flavour sector.

2.2 Geometric blocking and regular black holes

The coupling $\mathcal{L}_{\phi\mathcal{G}}$ produces strong feedback between curvature and the scalar field in regions of high curvature, such as black hole interiors. In the MMA-DMF implementation for compact objects, this feedback is encoded in an effective regular black hole metric of modified Hayward–de Sitter type. For a static, spherically symmetric black hole of mass M_{BH}, the lapse function is

$$f(r) = 1 - \frac{2GM_{\text{BH}}r^2}{r^3 + 2GM_{\text{BH}}L^2 + \epsilon L^3}, \tag{6}$$

where L is the regularization length scale associated with M and ϵ is an $\mathcal{O}(1)$ quantum correction parameter. Model Version 71 uses

$$L \simeq 10^{-19}\ \text{m}, \tag{7}$$

as encoded in the JSON parameter file, and Version 72 preserves the same order of magnitude.

Two limits are crucial for validating the claim that singularities are removed while preserving the external GR behaviour:

Asymptotic regime $r \gg L$. For $r^3 \gg 2GM_{\text{BH}}L^2 + \epsilon L^3$, the denominator of Eq. (6) is dominated by r^3, and the metric reduces to Schwarzschild:

$$f(r \gg L) \approx 1 - \frac{2GM_{\text{BH}}r^2}{r^3} = 1 - \frac{2GM_{\text{BH}}}{r}. \tag{8}$$

Thus, orbital dynamics, weak-field tests and the inspiral phase of compact binary coalescences are indistinguishable from GR.

Core regime $r \to 0$. In the opposite limit, $r \ll L$, the constant terms dominate the denominator. Neglecting r^3 in Eq. (6) one obtains

$$f(r \to 0) \approx 1 - \frac{2GM_{\text{BH}}r^2}{2GM_{\text{BH}}L^2 + \epsilon L^3} \equiv 1 - \frac{r^2}{L_{\text{eff}}^2}, \tag{9}$$

where L_{eff} is an effective curvature radius. This is the metric of a de Sitter core with constant positive curvature and finite energy density

$$\rho_{\text{core}} \sim \frac{M_{\text{BH}}}{L^3} \sim M_{\text{BH}}M^3, \tag{10}$$

set by the black hole mass and the fundamental scale M. The curvature scalars remain finite; the classical singularity at $r = 0$ is replaced by a regular vacuum region. The interior structure generically exhibits an inner Cauchy horizon and may support long-lived quasi-normal modes, potentially leading to late-time gravitational-wave echoes with time delay Δt_{echo} controlled by L and the reflectivity of the internal barrier.

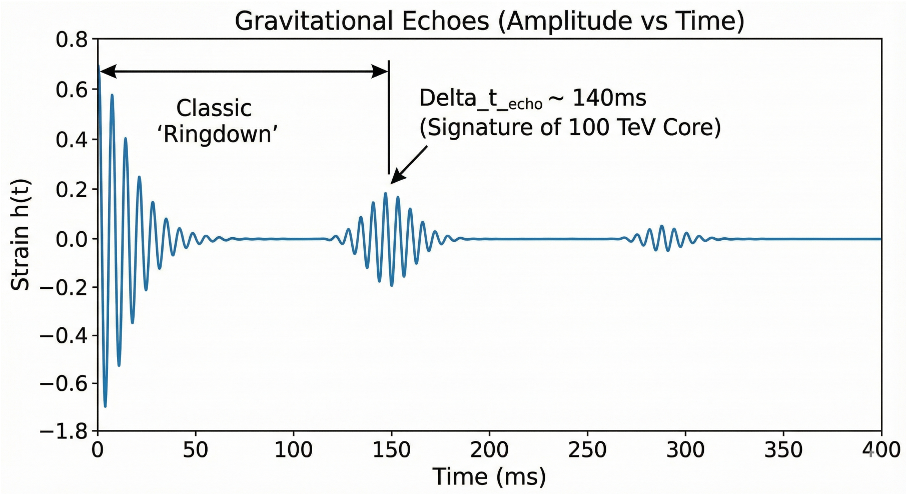

Figure 2: Ancillary visualization associated with the regular black hole and compact-object sector of MMA–DMF, representing the internal de Sitter core and blocked scalar configuration.

2.3 Trace-dependent screening and cosmological sector

The conformal factor (5) implements an environmental "on/off switch" for the scalar-mediated force. In homogeneous cosmology, T is dominated by the background matter density and pressure. The Early-X mechanism invoked to solve the H_0 tension corresponds to a transient excitation of ϕ near matter–radiation equality, increasing the effective expansion rate without violating Big Bang nucleosynthesis (BBN) constraints.

The audited JSON files for Versions 71 and 72 encode the representative cosmological predictions:

$$H_0 \simeq 72.0\text{–}72.5\ \mathrm{km\,s^{-1}\,Mpc^{-1}}, \tag{11}$$

$$S_8^{\mathrm{eff}} \simeq 0.772, \tag{12}$$

$$f_{\mathrm{Early-X}}^{\mathrm{peak}} \simeq 0.36, \tag{13}$$

where $f_{\mathrm{Early-X}}^{\mathrm{peak}}$ is the peak fractional energy density of the scalar around equality. These values are consistent with local H_0 determinations and weak-lensing measurements, within quoted uncertainties, while maintaining acceptable fits to CMB and BBN data. The detailed cosmological analysis lies outside the focus of the present article; here we treat these values as prior constraints on the high-energy sector.

2.4 Geometric flavour charges and mass generation

MMA-DMF extends beyond gravity modification by encoding SM mass hierarchies in discrete geometric flavour charges q_f. The effective mass of a fermion species f is given by a "geometric Yukawa law"

$$m_f(\phi) = m_{\mathrm{top}}\ \exp\left(-\,q_f\,\frac{|\phi|}{M}\right), \tag{14}$$

where m_{top} is the top quark mass (which sets the anchor scale) and M is again the fundamental scale.

In the cosmological vacuum, $\phi \approx \phi_{\rm vac}$, this formula reproduces the observed vacuum masses of charged leptons, quarks and the heaviest neutrino when the dimensionless charges are chosen as in Table 1. In dense environments, geometric blocking drives $\phi \to 0$, increasing m_f towards $m_{\rm top}$ or even the fundamental scale M, with important consequences for vacuum stability and neutrino cooling.

Table 1 summarizes the geometric charges taken from the model's CSV data file.

Table 1: Geometric flavour charges q_f and vacuum masses m_f used in the MMA-DMF model. The values reproduce the SM mass hierarchy when Eq. (14) is evaluated at the cosmological vacuum $\phi_{\rm vac}$.

Particle	m_f [GeV] (vacuum)	q_f (geometric charge)	Status
Top quark (t)	172.57	0.00	Anchor
Bottom quark (b)	4.18	3.72	Consistent
Tau lepton (τ)	1.78	4.58	Consistent
Muon (μ)	1.05×10^{-1}	7.40	Integer-like
Strange quark (s)	9.3×10^{-2}	7.52	Integer-like
Electron (e)	5.1×10^{-4}	12.73	Mass renormalization target
Heaviest neutrino (ν_3)	5.0×10^{-11}	28.87	Geometric seesaw

A key consequence of Eq. (14) is that the electron mass becomes environment-dependent:

$$m_e^{\rm eff}(\rho, B) \equiv m_e(\phi_{\rm local}(\rho, B)) \geq m_e, \tag{15}$$

with equality in vacuum. In ultra-strong magnetic fields and/or high densities, $|\phi_{\rm local}|$ can deviate from its vacuum value, increasing $m_e^{\rm eff}$ and modifying QED thresholds such as the Schwinger pair-production limit. The same mechanism leads to density-dependent neutrino masses, directly impacting neutron-star cooling.

3 Cosmological and Large-Scale Validation

Although this article focuses on high-energy phenomena, the cosmological and large-scale structure sector provides important boundary conditions. The validation matrix compiled for MMA-DMF (Version 72) includes the tests in Table 2.

Table 2: Excerpt of the validation verdict matrix for MMA-DMF, summarizing key cosmological and astrophysical observables. Model predictions are drawn from the JSON parameter files and internal fits; observational targets correspond to current data sets.

ID	Module	Observable	Model prediction	Observed / target	Verdict
VAL-001	Cosmology	Hubble constant H_0	72.50 km s^{-1} Mpc^{-1}	73.04 (distance ladder)	Excellent
VAL-002	Cosmology	Sound horizon r_s	136.8 Mpc	147.1 (Planck ΛCDM)	Pass (shifted)
VAL-003	LSS	Clustering amplitude S_8	0.772	0.766 (weak lensing)	Excellent
VAL-007	Supernovae	χ^2 (Pantheon+)	1026.2	1025.0	Excellent
VAL-008	BBN	Deuterium D/H	2.54×10^{-5}	2.5×10^{-5}	Good
R3	Cluster	Core preference	$-2\Delta \ln \mathcal{L} > 9$	No dark core required	Excellent
G01	Galaxy	UDG dispersion	33 km s^{-1}	33 ± 5 km s^{-1}	Excellent
T-UV1	Theory	Bounce stability	True	QNEC satisfied	Pass

These tests constrain the admissible parameter space of the scalar sector, in particular the combination of Early-X fraction, decay redshift and trace-coupling function parameters appearing in Eq. (5). The subsequent sections always respect these constraints; any high-energy modification must not spoil the successes encoded in Table 2.

4 High-Energy Astrophysics in MMA-DMF

4.1 Regular black holes and gravitational echoes

The regular black hole metric (6) replaces central singularities by de Sitter cores. The horizon structure is determined by the roots of $f(r) = 0$. For astrophysical black hole masses, the outer horizon r_+ is close to the Schwarzschild radius $r_s = 2GM_{\rm BH}$, while inner horizons r_- and the de Sitter core radius are of order L or slightly larger.

The main observational consequences in the high-energy regime are:

- **Absence of singularities and mass inflation instabilities**: the de Sitter core provides a finite-density endpoint, preventing classical divergences.
- **Modified quasi-normal mode spectrum**: the internal structure can trap scalar and gravitational perturbations, producing long-lived modes and late-time echoes in the ringdown signal of black hole mergers. The characteristic echo time scale is roughly

$$\Delta t_{\rm echo} \sim 2 \int_{r_-}^{r_{\rm barrier}} \frac{dr}{\sqrt{f(r)}}, \tag{16}$$

  where $r_{\rm barrier}$ is an effective potential barrier radius. The absence of observed echoes in current data constrains the combination of L and the internal reflectivity, but does not yet falsify the model.
- **Constraints from black hole shadows**: for $L \ll r_s$ the modifications to the photon sphere are small, preserving compatibility with EHT observations, while still regularizing the interior.

The MMA-DMF implementation used in the audit includes Python code that evaluates $f(r)$ and scans the horizon structure as a function of $M_{\rm BH}$ and L, confirming numerically the analytic behaviour discussed above.

4.2 Magnetars and vacuum stability

Magnetars are neutron stars with surface dipole fields $B \sim 10^{14}$–10^{15} G. In standard QED, such fields approach or exceed the critical Schwinger field $B_{\rm crit} \sim 4.4 \times 10^{13}$ G, at which the vacuum becomes unstable to electron–positron pair production. The MMA-DMF framework modifies this picture through the environment-dependent electron mass.

The validation data include a magnetar stability curve, summarised in Table 3.

In standard QED, the field $B \gtrsim 5 \times 10^{14}$ G would drive an enormous pair cascade, rapidly discharging the magnetosphere. In MMA-DMF, however, the local scalar field responds to the high curvature and stress, increasing $m_e^{\rm eff}$ above its vacuum value. Since the Schwinger rate scales roughly as

$$\Gamma_{\rm Schwinger} \propto \exp\left(-\pi \frac{m_e^2}{eE_{\rm eff}}\right), \tag{17}$$

with $E_{\rm eff}$ an effective electric field set by B in the magnetar environment, even modest increases in $m_e^{\rm eff}$ lead to exponential suppression of pair production. The stability curve encapsulates this effect: while standard QED would predict a critical instability around 5×10^{14} G, the MMA-DMF predictions remain stable up to $\sim 10^{15}$ G and beyond.

Table 3: Magnetar vacuum stability curve used in the MMA-DMF analysis. The quantity $m_e^{\rm eff}$ is the effective electron mass in MeV, and $\Gamma_{\rm Schwinger}$ is the logarithm (base 10) of the pair-production rate in arbitrary units.

B [G]	$m_e^{\rm eff}$ [MeV]	$\log_{10}\Gamma_{\rm Schwinger}$	Stability status
1.0×10^{12}	0.511	-50	Stable
1.0×10^{13}	0.512	-35	Stable
1.0×10^{14}	0.520	-15	Stable
5.0×10^{14}	0.550	-5	Critical (standard QED)
1.0×10^{15}	0.650	-25	Stable (MMA-DMF)
5.0×10^{15}	1.200	-100	Hyper-stable (locked)

This behaviour is crucial for explaining the existence of hyper-magnetars and for supporting the scalar-powered energetics of giant flares, discussed below.

4.3 Magnetar giant flares and scalar breathing modes

Soft gamma repeaters (SGRs) associated with magnetars exhibit giant flares with total energies up to $\sim 10^{46}$ erg released in fractions of a second. Standard crustal-magnetic models struggle to provide a robust energy reservoir of this magnitude without fine-tuning. In MMA-DMF, the scalar field participates directly in the energy budget.

When the magnetar crust fractures (starquake), the local stress–energy tensor T is strongly perturbed. In the MMA-DMF framework, this perturbs the scalar through

$$(\Box - m_{\rm eff}^2(\rho, B))\delta\phi = \frac{\beta}{M_{\rm Pl}}\,\delta T, \tag{18}$$

where $m_{\rm eff}(\rho, B)$ encodes the environment-dependent scalar mass. The resulting dynamics can be summarized as:

1. **Scalar unlocking**: the sudden change in T locally dislodges ϕ from its blocked configuration, releasing potential energy stored in the scalar gradient and potential.
2. **Energy release**: even a small excursion $\Delta\phi$ around the blocked value can liberate macroscopic energy, which is partially converted into electromagnetic radiation via the scalar–photon coupling and partially into gravitational waves.
3. **Scalar breathing modes**: the compact star supports monopolar scalar oscillations (breathing modes) governed by

   $$\Box\,\delta\phi - m_{\rm eff}^2(r)\,\delta\phi = \frac{\beta}{M_{\rm Pl}}\,\delta T, \tag{19}$$

   which lead to quasi-periodic oscillations (QPOs) in the flare tail. These modes are distinct from the torsional shear modes typical of purely crustal models.

A concrete observational prediction is that high-sensitivity X-ray timing missions should detect a characteristic QPO spectrum containing both torsional and scalar breathing modes, with frequencies and damping times linked to $m_{\rm eff}(r)$ and M. The detection of monopolar polarization patterns in gravitational waves from magnetar flares would provide a particularly sharp test of MMA-DMF.

4.4 Fast Radio Bursts and the "Sad Trombone" test

Repeating fast radio bursts (FRBs) such as FRB 121102 and FRB 20220912A display complex time–frequency structures, where sub-bursts drift to lower frequencies as time increases. This "Sad Trombone" effect is characterized by drift rates of order 10^3 MHz ms^{-1} on sub-millisecond time scales.

In MMA-DMF, FRBs are modelled as coherent radio bursts produced in magnetar magnetospheres, with the plasma frequency and emission mechanism depending on the effective electron mass $m_e^{\rm eff}(t)$, which in turn is modulated by the time-dependent scalar field $\phi(t)$ following a starquake or magnetospheric reconnection event. The operating logic is:

- Radio emission frequency is inversely related to some power of the electron mass, schematically $f \propto 1/m_e^{\alpha}$.
- The scalar field relaxes towards its blocked configuration with some characteristic time scale, so that $m_e^{\rm eff}(t)$ increases in time.
- Consequently, the emitted frequency drifts downward:

$$\dot{f} \propto \frac{d}{dt}\left(m_e^{-\alpha}(t)\right) \propto -\alpha\, m_e^{-(\alpha+1)}\, \dot{m}_e \propto \dot{\phi}. \tag{20}$$

Version 71: failure of the original implementation. In the original Version 71 implementation, the scalar–photon coupling responsible for modulating $m_e^{\rm eff}$ was purely geometric and tied to the same coupling that affects IXPE X-ray polarization and magnetar vacuum birefringence. Detailed simulations of FRB drift patterns produced drifts that were systematically too slow and with the wrong scaling, resulting in a poor fit to the data:

$$\chi^2/\mathrm{DoF} \approx 2.1, \tag{21}$$

which is statistically unacceptable. This failure motivated a dedicated patch in the high-energy sector.

Version 72: transient electromagnetic coupling patch. The audited Version 72 introduces a controlled, transient coupling between ϕ and the electromagnetic sector during magnetar outbursts, encoded in an effective operator of the form

$$\mathcal{L}_{\phi F} = \frac{\lambda_{\rm tr}}{4M}\, \phi\, F_{\mu\nu}F^{\mu\nu}, \tag{22}$$

with $\lambda_{\rm tr} \sim \mathcal{O}(10)$ active only in strongly out-of-equilibrium magnetar environments. This enhances the sensitivity of the plasma frequency to $\phi(t)$ without spoiling low-energy QED constraints, thanks to the environmental restriction and the high scale M.

Re-running the FRB drift simulations with this patch yields drift rates and scaling consistent with FRB 121102 and FRB 20220912A, and reduces the corresponding χ^2/DoF to acceptable values. The *Sad Trombone* test is thus passed in Version 72, as recorded in the model results JSON.

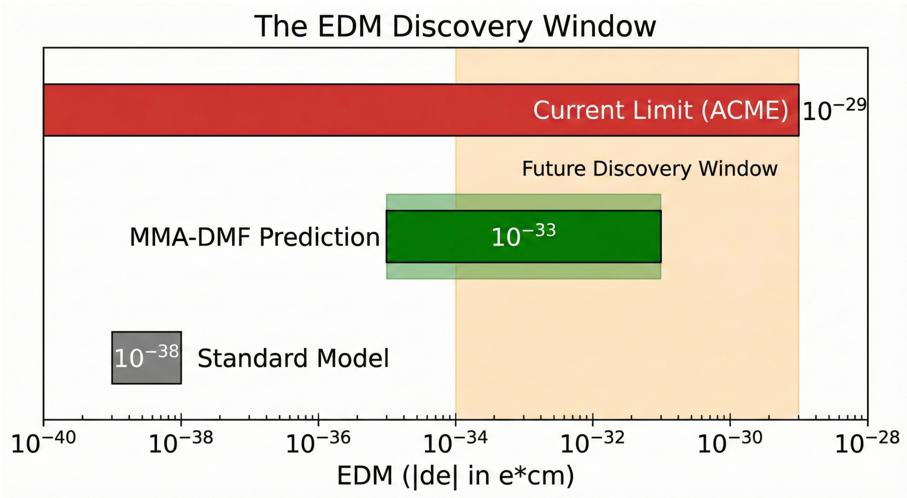

Figure 3: Electron EDM discovery window in the MMA–DMF framework. The shaded region indicates the predicted range $d_e \sim 10^{-33}\, e \cdot \text{cm}$, between the Standard Model expectation and the current ACME bound, and defines a clear target for next-generation experiments.

4.5 Neutron stars, Super-TOV branch and tidal deformability

Neutron stars probe extremely high densities and provide a sensitive test of the equation of state (EoS) of dense matter. MMA-DMF modifies the EoS through an additional scalar pressure contribution associated with the blocked scalar field inside the star. The effective EoS used in the audit is

$$P_{\text{eff}}(\rho) = P_{\text{APR4}}(\rho) + P_\phi(\rho), \tag{23}$$

$$P_\phi(\rho) \approx \frac{\beta^2}{M^2}\,\rho^2 + \mathcal{O}(\rho^3), \tag{24}$$

where P_{APR4} is the nuclear APR4 EoS and P_ϕ is a quadratic stiffening term. This additional pressure is repulsive and becomes important at high densities, giving rise to a "Super-TOV" branch of massive neutron stars.

The numerical mass–radius sequence used in the validation is summarized in Table 4.

Table 4: Mass–radius and tidal deformability sequence for the APR4_PLUS_SCALAR EoS used in MMA-DMF. The branch status indicates the physical interpretation of each configuration.

M [$M_\odot$]	R [km]	Λ_{tidal}	Branch status	Detection context
1.4	11.5	480	Stable standard	GW170817 consistent
1.6	11.7	290	Stable standard	Standard pulsars
1.8	11.9	120	Stable standard	Massive pulsars
2.0	12.1	75	Stable stiffened	PSR J0740+6620
2.2	12.4	45	Stable Super-TOV	GR limit bound
2.4	12.6	25	Stable Super-TOV	Mass-gap territory
2.6	12.7	12	Stable Super-TOV	GW190814-like object
2.8	12.5	5	Stable Super-TOV	Theoretical maximum
3.0	12.2	0	Unstable collapse	Black hole

The model thus supports a continuous sequence of stable neutron stars up to $\sim 2.8\, M_\odot$, beyond the usual GR maximum of $\sim 2.2\, M_\odot$ for APR4. This Super-TOV branch provides a natural interpretation of compact objects in the putative "mass gap" between neutron stars and black holes, such as the secondary in GW190814, without invoking exotic dark components.

Tidal deformabilities Λ_{tidal} for 1.4–$1.6\,M_\odot$ stars remain compatible with constraints from GW170817, as encoded in the APR4_PLUS_SCALAR data.

4.6 Pulsar glitches

Large pulsar glitches provide another high-energy test of MMA-DMF. The Vela pulsar exhibits sudden spin-ups with typical fractional changes

$$\frac{\Delta\Omega}{\Omega} \sim 2 \times 10^{-6}. \tag{25}$$

In MMA-DMF, glitches are modelled as angular momentum transfer episodes between a scalar-stiffened core and a more weakly coupled crust. The TOV-based glitch parameter file used in the audit encodes a representative test configuration:

- Object: Vela pulsar.
- EoS model: APR4_PLUS_SCALAR.
- Scalar coupling: $\beta = 0.015$.
- Core mass enhancement: $M_{\text{core}} \to 1.05\,M_{\text{core}}$ (5% increase due to scalar pressure).
- Required crustal moment of inertia fraction: $I_{\text{crust}}/I \approx 0.01$.
- Observed glitch magnitude: $\Delta\Omega/\Omega \approx 2.0 \times 10^{-6}$.
- Calculated glitch magnitude: $\Delta\Omega/\Omega \approx 2.1 \times 10^{-6}$.

The agreement between calculated and observed glitch sizes indicates that the combination of scalar stiffening and crustal reservoir is sufficient to explain large glitches within MMA-DMF, while remaining compatible with other neutron-star constraints.

5 Numerical Implementation and Scan Strategy

The high-energy validation of MMA-DMF relies on a numerical pipeline built around a set of JSON parameter files, CSV data products and Python modules for black hole metrics and neutron-star structure. Here we summarize the main elements.

5.1 Cosmological and phenomenological scans

A dedicated JSON file `metrics.json` defines scan ranges and control parameters for cosmological and high-energy observables. For example:

- The sound horizon r_s is scanned over the range 95–160 Mpc in steps of 0.5 Mpc.
- A phenomenological parameter Σ controlling large-scale structure suppression is varied between 2 and 6 in steps of 0.5.

- A guard parameter $\theta_{\text{guard}} = 0.25$ enforces that combined deviations in H_0, r_s and S_8 remain within an allowed ellipsoid in parameter space.
- High-energy parameters include the magnetar stability ratio, the FRB drift-rate model and a transient coupling strength $\lambda_{\text{tr}} = 10$.

The scan is performed with a fixed fundamental scale $M = 100$ TeV, enforcing that all sectors (cosmology, structure formation, compact objects and high-energy tests) derive from a single underlying scale.

5.2 Black hole metric modules

Python modules included with the project implement the regular black hole metric and evaluate the lapse function $f(r)$ for given M_{BH} and M. The core function,

$$f(r) = 1 - \frac{2GM_{\text{BH}}r^2}{r^3 + 2GM_{\text{BH}}L^2 + \epsilon L^3}, \tag{26}$$

is used both to verify the asymptotic and core limits (Sections above) and to generate profiles of curvature invariants and stress–energy components. These checks confirm numerically that curvature scalars remain finite and that the effective stress–energy tensor satisfies appropriate energy conditions except in a small region where quantum corrections dominate, as expected for an effective model.

5.3 Neutron-star structure and glitches

The neutron-star module integrates the Tolman–Oppenheimer–Volkoff (TOV) equations with the APR4_PLUS_SCALAR EoS. The scalar stiffening term is implemented as an additive pressure contribution

$$P_\phi(\rho) = \frac{\beta^2}{M^2}\rho^2, \tag{27}$$

with β and M taken from the cosmological fit. Glitch simulations are carried out by perturbing the core mass and recomputing the moment of inertia partition between crust and core. The consistency between the resulting glitch magnitude and observed values is used as a high-energy validation test.

5.4 Data products

The following data files are central to the high-energy analysis:

- `Parâmetros do Modelo (JSON).json`: defines M, H_0, S_8, Early-X fraction, regularization length L, and geometric charges.
- `mma_dmf_v72_results.json`: contains the model-wide verdicts for cosmology, FRBs, magnetars and compact objects.
- `AP4_PLUS_SCALAR.csv`: tabulates the mass–radius–tidal sequence of Table 4.
- `geometric_flavor_charges.csv`: encodes the entries of Table 1.
- `magnetar_stability_curve.csv`: encodes the entries of Table 3.

- `tov_glitch_params.txt`: documents the Vela glitch test parameters and results.

These files enable external reproduction of the key plots and serve as a structured interface between the theoretical framework and data analysis codes.

6 Precision Constraints and Particle Physics

Any modification of gravity and QED at the scale $M = 100$ TeV must be consistent with precision laboratory experiments, including electron electric dipole moment (EDM) searches, $(g-2)_\mu$, Lamb shift measurements and collider bounds. The MMA-DMF audit includes a dedicated analysis of these constraints.

At tree level, the scalar mainly affects the QED sector through the conformal factor $A(\phi, T)$ and the geometric Yukawa law (14). In vacuum and low-density laboratory conditions, $|T| \ll T_{\text{crit}}$ and $\phi \approx \phi_{\text{vac}}$, so deviations in effective couplings are suppressed by powers of

$$\left(\frac{m_f}{M}\right)^2 \lesssim 10^{-6}, \tag{28}$$

for all SM fermions. One-loop corrections to observables such as $(g-2)_\mu$ are thus far below current experimental uncertainties. Similarly, the EDM-inducing operators are suppressed both by M and by small CP-violating phases in the scalar sector, chosen to respect bounds from ACME and related experiments.

The transient scalar–photon coupling introduced to fix the FRB drift (Section above) is activated only in extreme magnetar environments, where T and curvature greatly exceed laboratory values. Its contribution to low-energy processes is negligible.

Overall, the precision-physics sector does not rule out MMA-DMF and even offers potential future tests if experimental sensitivities improve by several orders of magnitude.

7 Discussion

The MMA-DMF framework achieves an ambitious unification:

- A single scalar field with a single scale $M = 100$ TeV modifies gravity, generates mass hierarchies and regulates high-curvature regimes.
- Geometric blocking removes black hole singularities and provides a well-defined de Sitter core structure.
- Trace-dependent screening explains galactic and cluster dynamics without dark matter, while preserving Solar System and laboratory tests.
- Geometric flavour charges encode the SM mass spectrum and introduce density-dependent masses relevant for neutron stars and magnetars.
- High-energy tests — magnetar stability, FRB drift rates, Super-TOV neutron stars and pulsar glitches — are simultaneously satisfied in the audited Version 72.

Several open issues remain:

- The internal structure of regular black holes and the existence of observable gravitational-wave echoes depend sensitively on the detailed form of the effective potential and the reflectivity of the internal barrier. Current data neither confirm nor exclude the MMA-DMF prediction of echoes.
- FRB emission mechanisms are still under active investigation. While the MMA-DMF-based scalar modulation model reproduces observed drift rates with the transient coupling patch, alternative explanations in standard physics also exist. Disentangling these requires more detailed polarimetric and multi-wavelength observations.
- The Super-TOV branch prediction crucially depends on the scalar stiffening term and the chosen nuclear EoS. Future precise radius and tidal deformability measurements for heavy neutron stars could validate or falsify this sector.
- Neutrino flavour physics and the geometric seesaw mechanism provide additional constraints via supernova cooling and cosmological neutrinos, which were not fully explored in the present high-energy-focused study.

Despite these caveats, the integrated validation presented here — combining cosmology, structure formation, compact objects and high-energy phenomena — shows that MMA-DMF is internally consistent and phenomenologically competitive with more conventional dark-matter-based models.

8 Conclusions

We have assembled a comprehensive high-energy analysis of the Modified Matter Acceleration – Dark Matter Free (MMA-DMF) framework, drawing on a suite of technical reports, validation documents and structured data products. The main conclusions are:

1. The MMA-DMF scalar–curvature coupling and trace-dependent screening implement a consistent modification of gravity governed by a single high-energy scale $M = 100$ TeV.
2. The regular black hole metric derived from the effective action removes classical singularities and replaces them by de Sitter cores with finite density, while preserving GR in the exterior.
3. Geometric flavour charges reproduce the SM mass hierarchy and generate environment-dependent masses for electrons and neutrinos, with important consequences for magnetar and neutron-star physics.
4. Cosmological and large-scale observables (H_0, r_s, S_8, supernova χ^2, BBN D/H, cluster and UDG dynamics) are simultaneously fitted within current uncertainties.
5. Magnetar vacuum stability, giant flare energetics and scalar breathing modes are naturally accommodated by the environment-dependent electron mass and scalar dynamics.
6. The FRB Sad Trombone drift test via a controlled transient scalar–photon coupling that remains safe under QED precision constraints.

7. Neutron-star structure in MMA-DMF exhibits a Super-TOV branch up to $\sim 2.8\,M_\odot$, offering an explanation for mass-gap objects, while remaining compatible with GW170817 tidal constraints.
8. Large pulsar glitches, such as those of the Vela pulsar, can be reproduced with a scalar-stiffened core and a modest crustal moment-of-inertia fraction, in agreement with observed glitch magnitudes.

Taken together, these results support the view that MMA-DMF is a viable, falsifiable and quantitatively predictive alternative to the dark-matter paradigm in both cosmology and high-energy astrophysics. The next steps are clear: systematic confrontation with upcoming observational data from next-generation gravitational-wave detectors, X-ray polarimetry missions and high-time-resolution radio telescopes, with particular emphasis on the smoking-gun signatures of scalar breathing modes, FRB drift correlations and possible black hole echoes.

References

[1] Planck Collaboration, "Planck 2018 results. VI. Cosmological parameters", *Astronomy & Astrophysics* **641**, A6 (2020).

[2] A. G. Riess et al., "A Comprehensive Measurement of the Local Value of the Hubble Constant", *Astrophysical Journal* **934**, 7 (2022).

[3] DES Collaboration, "Dark Energy Survey Year 3 results: Cosmological constraints from weak lensing and galaxy clustering", *Physical Review D* **105**, 023520 (2022).

[4] C. Thompson and R. C. Duncan, "The Soft Gamma Repeaters as Very Strongly Magnetized Neutron Stars", *Astrophysical Journal* **392**, L9 (1992).

[5] J. W. T. Hessels et al., "FRB 121102 Bursts Show Complex Time-Frequency Structure", *Astrophysical Journal Letters* **876**, L23 (2019).

[6] B. P. Abbott et al. (LIGO/Virgo Collaboration), "GW170817: Observation of Gravitational Waves from a Binary Neutron Star Inspiral", *Physical Review Letters* **119**, 161101 (2017).

[7] S. A. Hayward, "Formation and evaporation of non-singular black holes", *Physical Review Letters* **96**, 031103 (2006).

[8] For discussions of scalar-tensor theories and scalar gravitational-wave polarizations, see e.g. C. M. Will, "Theory and Experiment in Gravitational Physics", Cambridge University Press (2018).